




Interfacial proximity and interplay between Kondo and short-range magnetic correlations in heterostructures

Julián Faúndez¹, Leonardo C. Prauchner², Peter S. Riseborough¹,

Sebastian E. Reyes-Lillo³, and Sergio G. Magalhaes²

¹*Physics Department, Temple University, Philadelphia, Pennsylvania, 19122, USA*

²*Instituto de Física, Universidade Federal do Rio Grande do Sul, Porto Alegre, RS, 91501-970, Brazil and*

³*Departamento de Ciencias Físicas, Universidad Andres Bello, Santiago 837-0136, Chile*

(Dated: May 10, 2024)

In this work, we investigate the influence of interlayer distance in a heterostructure containing both Kondo effects and short-range magnetic correlations. Our proposed heterostructure comprises three coupled square lattice layers. The first layer is governed by the Kondo-Heisenberg lattice model involving f - and d -electrons, which interact via Kondo and Heisenberg couplings, J_K and J_H , respectively. The other two layers consist of non-interacting itinerant electrons, where coupling with the first layer is determined by two perpendicular hopping parameters. We find that varying the interlayer couplings induces electronic dynamics at the interface, altering the behavior of mean-field parameters describing the Kondo effect and short-range magnetic correlations. The system's temperature - interlayer hopping parameter phase diagram exhibits a sequence of discontinuous and continuous transitions. In the cases, $|J_K| < |J_H|$ and $|J_K| > |J_H|$ rich phase diagrams are found which include Kondo, ferromagnetic and antiferromagnetic correlations. Our work provides insights into hosting Kondo correlations in heterostructures.

I. INTRODUCTION

In recent years, significant experimental advances have enabled the synthesis of ultrathin layers of heavy fermion electron systems, such as CeCoIn₅ and CeIn₃, [1–3]. Notably, superlattices or heterostructures can be artificially created by periodically stacking these layers, offering the possibility of modifying the electronic structure and stability of exotic phases. Heavy fermion heterostructures exhibit unique physical properties that are in general distinct from their individual counterparts, including novel states of matter such as magnetism, superconductivity, Kondo effect, the presence of short-range magnetic correlations and classical and quantum multicritical points [4–12]. Overall, the study of such structures provides a means of advancing our understanding of complex electronic systems and developing new technological applications [13–17].

Interestingly, artificial heterostructures have emerged combining different configurations of lattice geometries and layer materials [18–24]. In particular, the use of Kondo layers in heterostructures, such as CeIn₃/LaIn₃, has resulted in the development of a new class of materials known as Kondo heterostructures. These heterostructures are comprised of alternating layers of Kondo and non-magnetic materials [25–30].

Interface effects can influence the emergence or suppression of several phases, including the normal state (NS), the Kondo state (K) as well as ferromagnetic correlations (F_c) and antiferromagnetic correlations (AF_c) [25, 31]. For instance, the presence of interfaces can modulate the electronic density of states in adjacent layers, thereby affecting the formation of Kondo bound states [32]. Interlayer interactions can perturb local magnetic properties and spin dynamics, consequently suppressing the formation of a Kondo phase [33, 34]. Thus, inves-

tigating how the lattice geometry and composition of the heterostructure influence the formation and dynamics of electronic and magnetic states in the presence of interfaces is crucial for understanding Kondo heterostructures [31, 35, 36]. Kondo heterostructures have promising applications in the realm of nanoelectronics, including the creation of innovative spintronics devices. Moreover, they can be instrumental in the development of devices for quantum computing. Consequently, the dynamics of Kondo layers within heterostructures represents an intriguing domain within materials physics, offering the potential to unlock a plethora of new electronic functionalities [35, 37, 38].

A significant number of works have employed the Kondo lattice model within the fermionic mean-field approximation in a single layer, where ferromagnetic, antiferromagnetic, Kondo and mixed phases beyond the *half-filling* regime have been identified [39–41]. Moreover, studies on a bilayer with a in-situ attractive Hubbard model and Kondo interactions, have lead to the discovery of magnetic, Kondo and superconducting states [42]. Also, at zero temperature, it has been demonstrated that the competition between the Kondo effect and the RKKY interaction is influenced by the structure of two Kondo layers and a single metallic lattice, where the coupling between layers is given by a homogeneous hopping term t_z [43].

Furthermore, a phenomenon known as the *Nozières exhaustion problem* may arise in two-dimensional Kondo lattices. This phenomena occurs when conduction electrons are unable to fully screen all the localized spins, indicating a lower density of conduction electrons compared to localized spins. This issue can lead to the emergence of distinct states of matter, such as magnetic or superconducting phases [44, 45]

In this paper we study Kondo effects and short-range

magnetic correlations in a heterostructure at *half-filling* regime, composed by three interacting square layers, see Fig. 1. *Layer 1* is a Kondo-Heisenberg lattice (KHL) with Heisenberg and Kondo interactions, J_H and J_K , respectively. The itinerant part is given by d -electrons with hopping term t_d . *Layer 2* has itinerant states (c -electrons) and t_c hopping term. The coupling between c - and d -electrons is determined by the hopping term t_{12} . In *layer 3* the hopping of c -electrons is given by t_c and the coupling between c - and d -electrons is determined by the hopping term t_{13} . The two c -electron layers create a *sandwich* with the KHL and t_{12} and t_{13} can be different. Finally, with the variation of hopping terms and the mixing of the layers, we can study the proximity effects among interfaces in the Kondo state and short-range magnetic correlations of the Kondo-Heisenberg heterostructure in two limiting cases, $|J_k| < |J_H|$ and $|J_k| > |J_H|$.

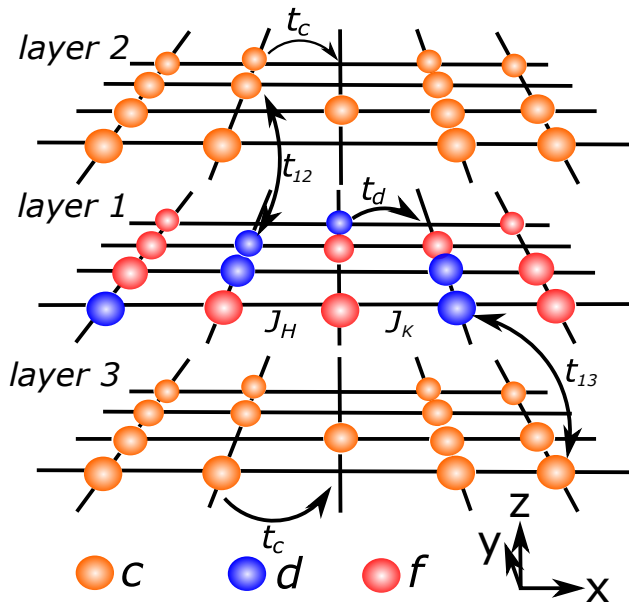


FIG. 1. Illustration of the heterostructure model with three interacting layers. In *layer 1*, the itinerant part of d -electrons is given by the hopping term t_d . J_H and J_K describe the Heisenberg and Kondo interactions, respectively. In *layer 2* there are itinerant states with c -electrons and hopping term t_c between neighborhoods. The coupling between c - and d -electrons is determined by the hopping term t_{12} . In *layer 3* the hopping of c -electrons is given by t_c and the coupling between c - and d -electrons is determined by the hopping term t_{13} . Furthermore, each layer has an specific bandwidth: $2W_d^1$, $2W_c^2$ and $2W_c^3$.

This article is organized as follow: the theory and model are given in section II. We find the Green's function that describe the most important self-consistent parameters: λ_{11} , Γ_{11} , σ_{12} and σ_{13} and their phase diagrams in the mean-field approximation. In section III we show the main numerical results: behaviors of mean-field parameters under proximity effects and the phase diagrams,

as well as relations to obtain the physical quantities of interest. Finally, in section IV we make a critical discussion of the main results.

II. THEORY AND MODEL

We aim to describe the proximity effect between three layers where, the first layer, denoted *layer 1*, has itinerant d - and localized f -electrons coupled through Kondo and Heisenberg interactions. The other two layers (*layer 2* and *layer 3*) are composed of non-interacting itinerant c -electrons. We also consider the hopping of electrons between d - and c -electrons among the three layers. This specific Kondo-Heisenberg heterostructure is shown in Fig. (1). The Hamiltonian that describes this heterostructure is composed of the following three terms

$$H = H_{\text{KHL}} + H_{\text{NIL}} + H_{\text{inter}}. \quad (1)$$

The term H_{KHL} corresponds to *layer 1* and it is given as

$$H_{\text{KHL}} = \sum_{\mathbf{k}\sigma} \epsilon_{d1}(\mathbf{k}) \hat{n}_{\mathbf{k}1\sigma}^d + E_0 \sum_{i\sigma} \hat{n}_{i1\sigma}^f - J_K \sum_i \hat{\mathbf{s}}_{d1i} \cdot \hat{\mathbf{S}}_{f1i} - J_H \sum_{\langle ij \rangle} \hat{\mathbf{S}}_{f1i} \cdot \hat{\mathbf{S}}_{f1j}. \quad (2)$$

Since we are interested in short-range magnetic correlations, the sum over $\langle i, j \rangle$ refers only to nearest-neighbor sites in *layer 1*. $\hat{n}_{\mathbf{k}1\sigma}^d = d_{\mathbf{k}1\sigma}^\dagger d_{\mathbf{k}1\sigma}$ with $d_{\mathbf{k}1\sigma}^\dagger$ ($d_{\mathbf{k}1\sigma}$) are creation (annihilation) operators of itinerant d -electrons with \mathbf{k} -momentum and spin σ , while $\hat{n}_{i1\sigma}^f = f_{i1\sigma}^\dagger f_{i1\sigma}$ with $f_{i1\sigma}^\dagger$ ($f_{i1\sigma}$) are creation (annihilation) operators of localized f -electrons with spin σ at site i . $\epsilon_1^d(\mathbf{k})$ is the dispersion relation for d -electrons. The third and fourth terms in H_{KHL} stand for the Kondo and Heisenberg interactions, respectively, with $J_K < 0$ and $J_H < 0$. The term H_{NIL} , corresponding to two normal layers with non-interacting itinerant c -electrons, is given as

$$H_{\text{NIL}} = \sum_{\mathbf{k}\sigma} \sum_{l=2}^3 \epsilon_c(\mathbf{k}) \hat{n}_{\mathbf{k}l\sigma}^c \quad (3)$$

where $\hat{n}_{\mathbf{k}l\sigma}^c = c_{\mathbf{k}l\sigma}^\dagger c_{\mathbf{k}l\sigma}$ and $c_{\mathbf{k}l\sigma}^\dagger$ ($c_{\mathbf{k}l\sigma}$) are the creation (annihilation) operator in layer $l = 1, 2$ with \mathbf{k} -momentum and spin σ . We assume a tight-binding conduction band for d - and c -electrons with bandwidth $2W_d$ and $2W_c$, respectively. Thus

$$\epsilon_{d(c)}(\mathbf{k}) = -\frac{W_{d(c)}}{2} \sum_{\mathbf{R}} \cos(\mathbf{k} \cdot \mathbf{R}) = -\frac{W_{d(c)}}{2} (\cos(k_x) + \cos(k_y)). \quad (4)$$

The coupling between the pairs of layers is given by a tight-binding model, and is expressed as

$$H_{\text{inter}} = -t_{12} \sum_{ij;\sigma} (d_{i1\sigma}^\dagger c_{j2\sigma} + c_{i2\sigma}^\dagger d_{j1\sigma}) - t_{13} \sum_{ij;\sigma} (d_{i1\sigma}^\dagger c_{j3\sigma} + c_{i3\sigma}^\dagger d_{j1\sigma}) \quad (5)$$

where d_{i1}^\dagger (d_{i1}) and $c_{i2(3)}^\dagger$ ($c_{i2(3)}$) are creation (annihilation) operators in site i of *layer 1*, *layer 2* and *layer 3*, respectively. We introduce the hermitian operators to describe the Kondo effect and short-range magnetic correlations [39, 40], which are given by

$$\hat{\lambda}_{i1\sigma} = \frac{1}{2N} (c_{i1\sigma}^\dagger f_{i1\sigma} + f_{i1\sigma}^\dagger c_{i1\sigma}),$$

$$\hat{\Gamma}_{ij1\sigma} = \frac{1}{2N} (f_{i1\sigma}^\dagger f_{j1\sigma} + f_{j1\sigma}^\dagger f_{i1\sigma}).$$

Thus, the spin-flipping part of Kondo and Heisenberg interactions is decoupled as

$$\hat{s}_{d1i}^x \hat{S}_{f1i}^x + \hat{s}_{d1i}^y \hat{S}_{f1i}^y = - \sum_{\sigma} \hat{\lambda}_{i1\sigma} \hat{\lambda}_{i1\bar{\sigma}}, \quad (6)$$

$$S_{f1i}^x S_{f1j}^x + S_{f1i}^y S_{f1j}^y = - \sum_{\sigma} \hat{\Gamma}_{ij1\sigma} \hat{\Gamma}_{ij1\bar{\sigma}}, \quad (7)$$

while the z components become

$$\hat{s}_{d1i}^z \hat{S}_{f1i}^z = 1/4 - \sum_{\sigma} (\hat{\lambda}_{i1\sigma})^2, \quad (8)$$

$$\hat{S}_{f1i}^z \hat{S}_{f1j}^z = 1/4 - \sum_{\sigma} (\hat{\Gamma}_{ij1\sigma})^2. \quad (9)$$

In Eqs. (8)-(9), the constraint $\hat{n}_{i1}^f = \hat{n}_{i1\uparrow}^f + \hat{n}_{i1\downarrow}^f = 1$ has been used explicitly.

We carry out a mean-field treatment of H_{KLL} which neglects quadratic fluctuations $\Delta \hat{\lambda}_{i1\sigma} = (\hat{\lambda}_{i1\sigma} - \lambda_{i1\sigma})$ and $\Delta \hat{\Gamma}_{ij1\sigma} = \hat{\Gamma}_{ij1\sigma} - \Gamma_{ij1\sigma}$ ($\langle \hat{\lambda}_{i1\sigma} \rangle = \lambda_{i1\sigma}$ and $\langle \hat{\Gamma}_{ij1\sigma} \rangle = \Gamma_{ij1\sigma}$). Moreover, we consider $\lambda_{i1\uparrow} = \lambda_{i1\downarrow} = \lambda_{11}$ and similarly $\Gamma_{ij1\uparrow} = \Gamma_{ij1\downarrow} = \Gamma_{11}$, i.e., translational invariant and since there is no magnetic long-range order, also symmetric up and down spin solutions. Therefore, for the Heisenberg term, as $\langle i, j \rangle$ refers to nearest neighbors, we get

$$(J_H \sum_{\langle ij \rangle} \hat{\mathbf{S}}_{f,i} \cdot \hat{\mathbf{S}}_{f,j})_{MF} = B \sum_{\mathbf{k}\sigma} \epsilon_d(\mathbf{k}) f_{\mathbf{k}\sigma}^\dagger f_{\mathbf{k}\sigma},$$

where

$$B = - \frac{4J_H \Gamma}{W^d}.$$

As a consequence, the 3-layer model mean-field Hamiltonian becomes

$$\begin{aligned} (\mathcal{H})_{MF} = & \sum_{\mathbf{k},\sigma} (B\epsilon_{d,1}(\mathbf{k}) + E_0) f_{\mathbf{k}1\sigma}^\dagger f_{\mathbf{k}1\sigma} + \sum_{\mathbf{k},\sigma} (\epsilon_{d,1}(\mathbf{k}) - \mu) d_{\mathbf{k}1\sigma}^\dagger d_{\mathbf{k}1\sigma} + \sum_{\mathbf{k},\sigma} (\epsilon_{c,2}(\mathbf{k}) - \mu) c_{\mathbf{k}2\sigma}^\dagger c_{\mathbf{k}2\sigma} \\ & + 2J_K \lambda_{11} \sum_{\mathbf{k},\sigma} (d_{\mathbf{k}1\sigma}^\dagger f_{\mathbf{k}1\sigma} + f_{\mathbf{k}1\sigma}^\dagger d_{\mathbf{k}1\sigma}) - t_{d1c2} \sum_{\mathbf{k},\sigma} (d_{\mathbf{k}1\sigma}^\dagger c_{\mathbf{k}2\sigma} + c_{\mathbf{k}2\sigma}^\dagger d_{\mathbf{k}1\sigma}) - t_{d1c3} \sum_{\mathbf{k},\sigma} (d_{\mathbf{k}1\sigma}^\dagger c_{\mathbf{k}3\sigma} + c_{\mathbf{k}3\sigma}^\dagger d_{\mathbf{k}1\sigma}) \\ & - 4J_k \lambda_{11}^2 - 2J_H \Gamma_{11}^2. \end{aligned} \quad (10)$$

Note that in Eq. (10), the Heisenberg interaction gives rise to a dispersion relation for the f -electrons, just as the Kondo interaction leads to effective hybridization between d - and f -electrons. In both cases, there is a dependence on temperature through Γ_{11} giving short-range magnetic correlations and λ_{11} that gives the global formation of Kondo singlets which, at high temperatures, can be expected to be null.

The 3-layer mean-field Hamiltonian given in Eq. (10) is replaced by

$$(\mathcal{H})_{MF} = \sum_{\mathbf{k}\sigma} \Psi_{\mathbf{k}\sigma}^\dagger \mathbf{h}_{\mathbf{k}} \Psi_{\mathbf{k}\sigma} - 4J_k \lambda_{11}^2 - 2J_H \Gamma_{11}^2, \quad (11)$$

where

$$\Psi_{\mathbf{k}\sigma} = \begin{pmatrix} f_{\mathbf{k}1\sigma} \\ d_{\mathbf{k}1\sigma} \\ c_{\mathbf{k}2\sigma} \\ c_{\mathbf{k}3\sigma} \end{pmatrix}$$

and

$$\mathbf{h}_{\mathbf{k}} = \begin{pmatrix} B\epsilon_{d1}(\mathbf{k}) + E_0 & 2J_k \lambda_{11} & 0 & 0 \\ 2J_k \lambda_{11} & \epsilon_{d1}(\mathbf{k}) & -t_{dc2} & -t_{dc3} \\ 0 & -t_{dc2} & \epsilon_{c,2}(\mathbf{k}) & 0 \\ 0 & -t_{dc3} & 0 & \epsilon_{c,2}(\mathbf{k}) \end{pmatrix}.$$

Using the results obtained in Eqs. (A2)-(A9), see Appendix A, the correlator λ_{11} , Γ_{11} , σ_{12} and σ_{13} can be

obtained self-consistently from the coupled equations

$$\lambda_{11} = \frac{1}{N} \sum_{\mathbf{k}} \oint \frac{dz}{2\pi i} f(z) \langle \langle d_{\mathbf{k},1\sigma} : f_{\mathbf{k},1,\sigma}^\dagger \rangle \rangle_z, \quad (12)$$

$$1 = \frac{J_H}{W^d} \frac{1}{N} \sum_{\mathbf{k}} \epsilon_d(\mathbf{k}) \oint \frac{dz}{2\pi i} f(z) \langle \langle f_{\mathbf{k},1\sigma} : f_{\mathbf{k},1,\sigma}^\dagger \rangle \rangle_z \quad (13)$$

and

$$\sigma_{12} = \frac{1}{N} \sum_{\mathbf{k}} \oint \frac{dz}{2\pi i} f(z) \langle \langle c_{\mathbf{k},2\sigma} : d_{\mathbf{k},1,\sigma}^\dagger \rangle \rangle_z, \quad (14)$$

$$\sigma_{13} = \frac{1}{N} \sum_{\mathbf{k}} \oint \frac{dz}{2\pi i} f(z) \langle \langle c_{\mathbf{k},3\sigma} : d_{\mathbf{k},1,\sigma}^\dagger \rangle \rangle_z. \quad (15)$$

The contour of the path integral in Eqs. (12) - (15) encircles the real axis without enclosing any poles of the Fermi-Dirac distribution. We also fix the total electronic density $n_t = (\langle \hat{n}_d \rangle + \langle \hat{n}_{c2} \rangle + \langle \hat{n}_{c3} \rangle)/3$ and the f -level E_0 using the chemical potential μ . To complete the self-consistency, the constraint $\hat{n}_f = 1$ is replaced by the mean field one $\langle \hat{n}_f \rangle = 1$.

III. RESULTS AND DISCUSSION

To simplify the complexity of numerical results, we consider the bandwidth given by: $W^d = W_{2(3)}^c = 1$. The density of states for both the d - and c -electrons is assumed to be semi-parabolic, and is given by

$$D(\omega) = \frac{3}{4}(1 - \epsilon^2) \quad |\epsilon| \leq 1. \quad (16)$$

The energies are measured in units of the half bandwidth to obtain dimensionless parameters and subsequently normalized by $t_c/W_{2(3)}^c$. In the following, to study the correlation effects in the heterostructure, we display the self-consistent solutions for the mean-field parameters given in Eqs. (12)-(15) versus the inter-layer hopping parameters t_{12}/t_c and t_{13}/t_c at *half-filling* regime, i.e., the occupation number of f -electrons in the KHI is $n^f = 1$, where $n^f = f_{\mathbf{k}1\sigma}^\dagger f_{\mathbf{k}1\sigma}$, $t_c = 1$ and $k_B = 1$.

We are interested in two limiting cases, $|J_K| < |J_H|$ and $|J_K| > |J_H|$. In the case $|J_H| > |J_K|$, the non-local coupling between f -electrons is much stronger than the non-local coupling between d - and f -electrons. In the case $|J_K| > |J_H|$, the non-local interactions between d - and f -electrons dominate over the non-local coupling of d -electrons, see Fig. 1. The relative size mean-field parameters Γ_{11}/t_c and λ_{11}/t_c indicate the relative the stability of the Kondo and short-range magnetic correlations. The quantities σ_{12}/t_c and σ_{13}/t_c describe the coupling between the layers conduction bands.

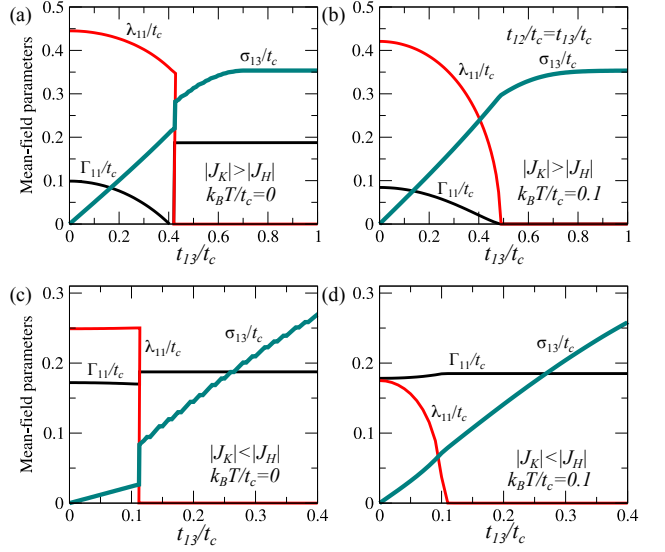


FIG. 2. Mean-field parameters λ_{11}/t_c , Γ_{11}/t_c and σ_{13}/t_c as functions of hopping parameter t_{13}/t_c , at the *half-filling* regime. (a) $J_K = -0.5$, and $J_H = -0.1$ at $k_B T/t_c = 0$, (b) $J_K = -0.5$, and $J_H = -0.1$ at $k_B T/t_c = 0.1$, (c) $J_K = -0.5$, and $J_H = -1$ at $k_B T/t_c = 0$ and (d) $J_K = -0.5$, and $J_H = -1$ at $k_B T/t_c = 0.1$. $W_{2(3)}^c = W^d = 1$. The hopping terms are equal to $t_{12}/t_c = t_{13}/t_c$. The behavior of σ_{12} is similar to σ_{13} .

A. Hopping dependence: $t_{12} = t_{13}$

In Fig. 2, we show the mean-field parameters Γ_{11}/t_c , λ_{11}/t_c , σ_{12}/t_c and σ_{13}/t_c as functions of hopping term $t_{12}/t_c = t_{13}/t_c$. In Figs. 2(a) and 2(c), the mean-field parameters, at $k_B T/t_c = 0$, are found for $|J_K| < |J_H|$ and $|J_K| > |J_H|$. In Figs. 2(b) and 2(d) the parameter λ_{11}/t_c decreases sharply at $t_{13}/t_c \approx 0.4$ and $t_{13}/t_c \approx 0.1$, respectively, disappearing for higher magnitudes of t_{13}/t_c . When $|J_K| < |J_H|$, the parameter Γ_{11}/t_c continuously decreases until reaching zero for $t_{13}/t_c \approx 0.4$ and remains constant for $t_{13}/t_c > 0.4$. In contrast, when $|J_K| > |J_H|$, Γ_{11}/t_c remains constant for all t_{13}/t_c but undergoes a sudden change at $t_{13}/t_c \approx 0.1$. The parameters σ_{12}/t_c and σ_{13}/t_c are equal and increase linearly but undergo an abrupt discontinuity at $t_{13}/t_c \approx 0.4$ and $t_{13}/t_c \approx 0.1$, continue to show a linear increase with t_{13}/t_c . In Figs. 2(b) and 2(d), the mean-field parameters at $k_B T/t_c = 0.1$ are shown for $|J_K| < |J_H|$ and $|J_K| > |J_H|$, respectively. When $|J_K| < |J_H|$, the parameters Γ_{11}/t_c and λ_{11}/t_c decreases quadratically at $t_{13}/t_c \approx 0.4$, while the parameters σ_{12}/t_c and σ_{13}/t_c are equal, i.e., $\sigma_{12}/t_c = \sigma_{13}/t_c$, increasing linearly until stabilizing and becoming constants for high values of t_{13}/t_c . When $|J_K| > |J_H|$, the parameter λ_{11}/t_c continuously decreases at $t_{13}/t_c \approx 0.1$, the parameter Γ_{11}/t_c is constant and independent of t_{13}/t_c , while $\sigma_{12}/t_c = \sigma_{13}/t_c$ are increasing linearly with the increase of t_{13}/t_c .

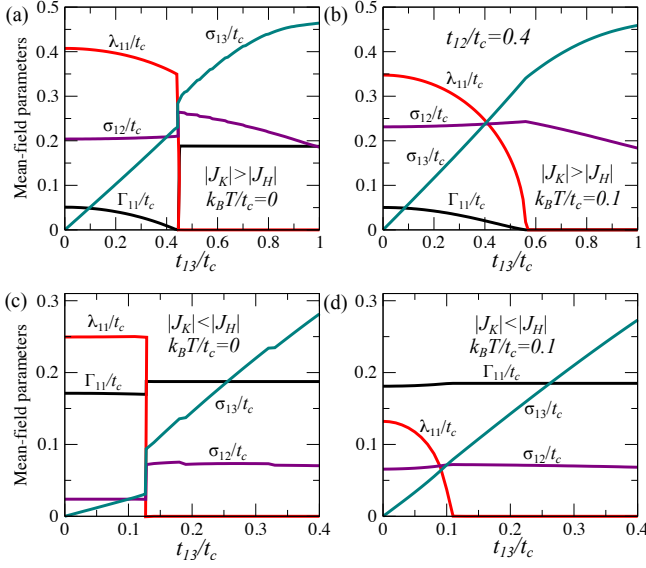


FIG. 3. Mean-field parameters λ_{11}/t_c , Γ_{11}/t_c , σ_{12}/t_c and σ_{13}/t_c as functions of hopping term t_{13}/t_c , for $n^f = 1$. (a) $J_K = -0.5$, and $J_H = -0.1$ at $k_B T/t_c = 0$, (b) $J_K = -0.5$, and $J_H = -0.1$ at $k_B T/t_c = 0.1$, (c) $J_K = -0.5$, and $J_H = -1$ at $k_B T/t_c = 0$ and (d) $J_K = -0.5$, and $J_H = -1$ at $k_B T/t_c = 0.1$. $W_{2(3)}^c = W^d = 1$. The hopping term $t_{12}/t_c = 0.4$.

B. Hopping dependence: $t_{12} \neq t_{13}$

Fig. 3 shows the mean-field parameters Γ_{11}/t_c , λ_{11}/t_c , σ_{12}/t_c , and σ_{13}/t_c as functions of the hopping term t_{13}/t_c , at $k_B T/t_c = 0$ and $k_B T/t_c = 0.1$. The hopping terms t_{12}/t_c and t_{13}/t_c differ, allowing the distances between *layer 1* and *layer 2* to be distinct from *layer 1* and *layer 3*. For simplicity, we had chosen $t_{12}/t_c = 0.4$. The behavior of the order parameters Γ_{11}/t_c and λ_{11}/t_c are essentially the same as shown in Fig. 2, but with different critical values of t_{13}/t_c . For $k_B T/t_c = 0$, shown in Figs. 3(a) and 2(c), the parameters σ_{12}/t_c and σ_{13}/t_c exhibit different behaviors. σ_{12}/t_c remains constant until $t_{13}/t_c \approx 0.4$, undergoes a small abrupt variation and subsequently decays linearly with increasing t_{13}/t_c . σ_{13}/t_c linearly increases, experiencing a discontinuity at $t_{13}/t_c \approx 0.4$, and subsequently continues to grow. When $|J_K| < |J_H|$, the behavior of σ_{12}/t_c is constant and independent of t_{13}/t_c , but experiences a slight discontinuity around $t_{13}/t_c \approx 0.1$. At $k_B T/t_c = 0.1$, as depicted in Figs. 3(b) and 3(d), when $|J_K| > |J_H|$, the parameter σ_{12}/t_c remains nearly constant until $t_{13}/t_c \approx 0.6$ and then decays linearly as t_{13}/t_c increases. The parameter σ_{13}/t_c increases for all values of t_{13}/t_c . When $|J_K| < |J_H|$, the parameter σ_{12}/t_c is nearly constant and independent of t_{13}/t_c , the parameter σ_{13}/t_c increase continuously for all values of t_{13}/t_c . In the following we show numerical results regarding the behavior of the mean-field parameters Γ_{11}/t_c and λ_{11}/t_c with the variation of the interlayer hopping terms.

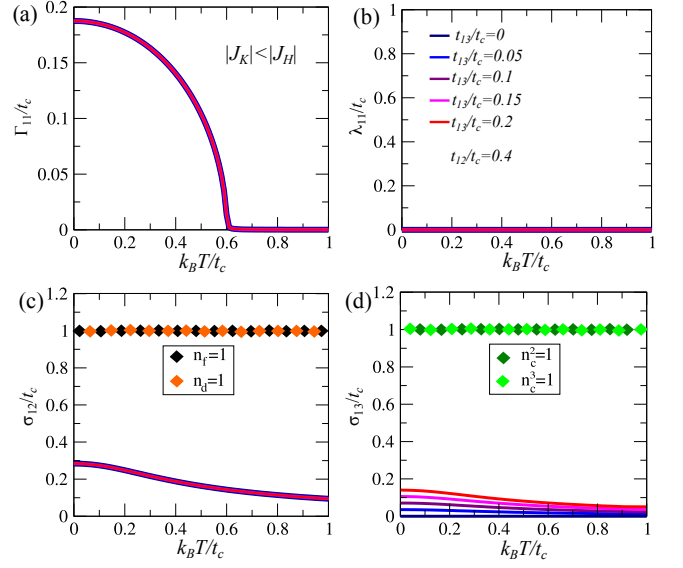


FIG. 4. Mean-field parameters (a) λ_{11}/t_c , (b) Γ_{11}/t_c , (c) σ_{12}/t_c and (d) σ_{13}/t_c as function of $k_B T/t_c$ under a variation of t_{13}/t_c for $n^f = 1$ and $n_t = (n_d + n_c^2 + n_c^3)/3 = 1$ in the case where the Heisenberg interaction is large compared to the Kondo coupling: $J_K = -0.5$, and $J_H = -1$. $W_{2(3)}^c = W^d = 1$ and the hopping parameter $t_{12}/t_c = 0.4$.

C. Temperature dependence: case $|J_K| < |J_H|$

Fig. 4 displays the mean-field parameters Γ_{11}/t_c , λ_{11}/t_c , σ_{12}/t_c , and σ_{13}/t_c as functions of $k_B T/t_c$, with varying hopping t_{13} . The hopping term between *layer 1* and *layer 2* is fixed at $t_{12}/t_c = 0.4$, maintaining a constant distance between these layers, while the distance between *layer 1* and *layer 3* varies, allowing for the finite variation of t_{13}/t_c . In Fig. 4(a), the behavior of the mean-field parameter Γ_{11}/t_c is shown as a function of $k_B T/t_c$ for finite values of t_{13}/t_c and $t_{12}/t_c = 0.4$. We can find that the behavior of Γ_{11}/t_c is independent of the values of t_{13}/t_c and quadratically decays around $k_B T/t_c \approx 0.6$. The mean-field parameter λ_{11}/t_c is zero in this case and is independent of t_{13}/t_c (see Fig. 4(b)). Figs. 4(c) and 4(d) show the parameters σ_{12}/t_c and σ_{13}/t_c , respectively, along with the occupation numbers of the *f*-, *d*-, and *c*-electrons in each of the three layers. The parameter σ_{12}/t_c asymptotically decays with increasing $k_B T/t_c$ and remains constant with respect to variations of t_{13}/t_c . The parameter σ_{13}/t_c also asymptotically decays with increasing $k_B T/t_c$, with a slight variations on changing t_{13}/t_c .

Fig. 5 shows the mean-field parameters Γ_{11}/t_c , λ_{11}/t_c , σ_{12}/t_c , and σ_{13}/t_c as functions of $k_B T/t_c$ under a finite variation of $t_{12}/t_c = t_{13}/t_c$ at $n^f = 1$ and $n_t = (n_d + n_c^2 + n_c^3)/3 = 1$. Similar to the previous result, Fig. 4(a), the self-consistent mean-field parameter Γ_{11}/t_c , Fig. 5(a), continuously decreases for all magnitudes of t_{12}/t_c , reaching vanishing small values at $k_B T/t_c = 0.6$, except for values below $k_B T/t_c \approx 0.1$ where a slight increment

is observed for $t_{12}/t_c < 0.15$. In Fig. 5(b), the mean-field parameter λ_{11}/t_c steadily decreases until completely disappearing around $k_B T/t_c \approx 0.1$ for magnitudes lower than $t_{13}/t_c < 0.15$, while for $t_{13}/t_c = 0.2$, the mean-field parameter λ_{11}/t_c is zero. In Figs. 5(c) and 5(d), the parameters σ_{12}/t_c and σ_{13}/t_c , with $\sigma_{12}/t_c = \sigma_{13}/t_c$, asymptotically decay for all values of $k_B T/t_c$ and t_{13}/t_c , while the occupation values of all electrons remain constant and equal to 1, i.e., $n^f = 1$.

D. Phase diagrams: case $|J_K| < |J_H|$

Although the mean-field parameters are not order parameters since they describe short-ranged correlations, they exhibit behavior akin to order parameters. Based on these parameters, we construct a phase diagram that does not indicate thermodynamic phase boundaries but, instead reflect the different correlations in the phases. The phase diagrams are constructed from Eqs. (12) and (13) for the mean-field parameters Γ_{11}/t_c and λ_{11}/t_c in the case $|J_K| < |J_H|$. In Fig. 6(a), we depict the phase diagram of $k_B T/t_c$ versus t_{13}/t_c , for a fixed value of $t_{12}/t_c = 0.4$, i.e., the interfaces of *layer 1* and *layer 3* are at a fixed distance. In this case, only short-range antiferromagnetic correlations AF_c are observed, independent of the value of t_{13}/t_c . For low values of t_{13}/t_c and as $k_B T/t_c$ decreases, a continuous transition (solid line) from a normal NS to AF_c is found, and as t_{13}/t_c starts to increase, for high values of $k_B T/t_c$, a continuous transition from AF_c to a NS is observed again. The absence of Kondo correlations is simply due to J_K being much lower than J_H . In addition, in Fig. 6(b), the phase diagram is shown when $t_{12}/t_c = t_{13}/t_c$. For low values of t_{13}/t_c and as $k_B T/t_c$ decreases, there is a continuous transition from NS to AF_c correlations. The "dome" corresponds to the coexistence of Kondo and AF_c . The "dome" shows that the Kondo correlations disappear continuously near $t_{13}/t_c = 0.15$. For $k_B T/t_c$ higher than $t_{13}/t_c > 0.13$, only AF_c correlations exist, regardless of the value of t_{13}/t_c .

E. Temperature dependence: case $|J_K| > |J_H|$

Fig. 7 depicts the mean-field parameters Γ_{11}/t_c , λ_{11}/t_c , σ_{12}/t_c and σ_{13}/t_c as function of $k_B T/t_c$ under varying hopping parameter t_{13}/t_c , for $n^f = 1$ and $n_t = (n_d + n_c^2 + n_c^3)/3 = 1$. In the case $|J_K| > |J_H|$, the hopping term between the *layer 1* and *layer 2* is fixed at $t_{12}/t_c = 0.4$, maintaining a constant distance between these layers, while the distance between the *layer 1* and *layer 2* varies, allowing for the finite variation of t_{13}/t_c . In Fig. 7(a), the behavior of the mean-field parameter Γ_{11}/t_c , with respect to $k_B T/t_c$ is shown under the variation of t_{13}/t_c . A discontinuity in Γ_{11}/t_c is observed for estimated values of $0.525 < t_{13}/t_c < 0.7$ at $k_B T/t_c \approx 0.01$ and $k_B T/t_c \approx 0.05$. The negative signal in Γ_{11}/t_c indicates that the spin correlation between the neighboring

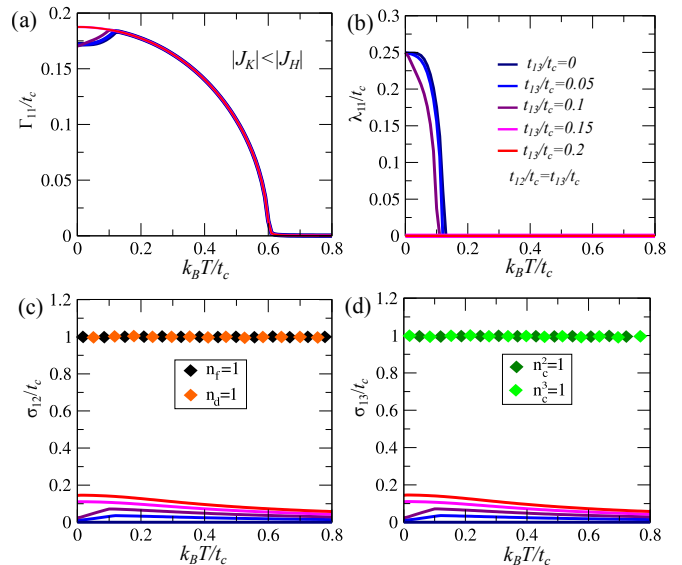


FIG. 5. Mean-field parameters (a) λ_{11}/t_c , (b) Γ_{11}/t_c , (c) σ_{12}/t_c and (d) σ_{13}/t_c as function of $k_B T/t_c$ under a variation of t_{13}/t_c for $n^f = 1$ and $n = (n_d + n_c^2 + n_c^3)/3 = 1$ in the case where the Heisenberg interaction is large compared to the Kondo coupling: $J_K = -0.5$, and $J_H = -1$. $W_{2(3)}^c = W^d = 1$ and the hopping parameters are $t_{12}/t_c = t_{13}/t_c$.

sites became ferromagnetic and when Γ_{11}/t_c goes to zero the spin correlations at different sites will become zero, since the spins are decoupled. The next effect is similar to varying from an antiferromagnetic state to a ferromagnetic state [40]. Furthermore, the mean-field parameter λ_{11}/t_c as a function of $k_B T/t_c$ is depicted in Fig. 7(b). For $t_{13}/t_c < 0.525$, λ_{11}/t_c continuously decreases until it reduces to zero. Conversely, for $t_{13}/t_c = 0.525$, λ_{11}/t_c is absent for low $k_B T/t_c$ values and abruptly increases around $k_B T/t_c \approx 0.01$. Specifically, for $t_{13}/t_c = 0.7$, a small region, or "dome" where λ_{11}/t_c exist is shown. Figs. 7(c) and 7(d) display the parameters σ_{12}/t_c , σ_{13}/t_c , and the respective occupation numbers of the *f*-, *d*-, and *c*-electrons in each of the three layers. We note that $\sigma_{12}/t_c \neq \sigma_{13}/t_c$ due to the constant distance between *layer 1* and *layer 2*, while the distance between *layer 1* and *layer 3* varies. Despite the differences in magnitude, both parameters asymptotically decay for high $k_B T/t_c$ values.

The self-consistent mean-field parameters Γ_{11}/t_c , λ_{11}/t_c , σ_{12}/t_c , and σ_{13}/t_c as functions of $k_B T/t_c$ for finite hopping term values, $t_{12}/t_c = t_{13}/t_c$ are depicted in Fig. 8 for the case $|J_K| > |J_H|$. The parameter Γ_{11}/t_c , Fig. 8(a), diminishes at lower $k_B T/t_c$ values. Specifically, at $t_{13}/t_c = 0.525$, a strong discontinuity occurs at a $k_B T/t_c \approx 0.045$. The parameter λ_{11}/t_c , depicted in Fig. 8(b), as the value of t_{13}/t_c increases, diminishes at lower $k_B T/t_c$ values. Specifically, at $t_{13}/t_c = 0.525$ (the same value of t_{13}/t_c that causes the discontinuity in Γ_{11}/t_c), the parameter λ_{11}/t_c only exists between $0.045 < k_B T/t_c < 0.085$. When $t_{13}/t_c = 0.7$, the param-

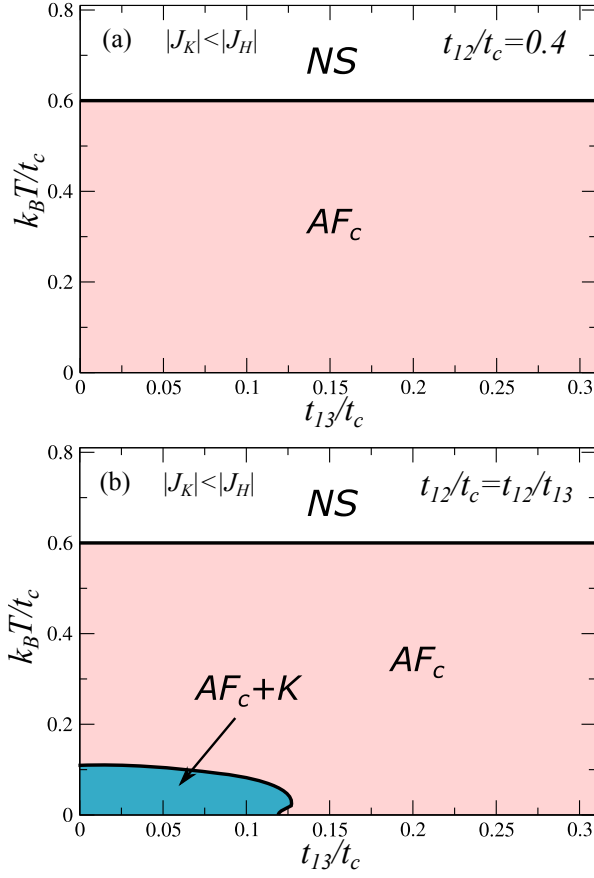


FIG. 6. Phase diagrams of $k_B T/t_c$ versus t_{13}/t_c with (a) $t_{12}/t_c = 0.4$ and (b) $t_{12}/t_c = t_{13}/t_c$ in the case where the Heisenberg interaction is large compared to the Kondo coupling: $J_K = -0.5$, and $J_H = -0.1$. $W_{2(3)}^c = W^d = 1$. NS is a normal state, F_c are ferromagnetic correlations and K is a Kondo state.

eter λ_{11}/t_c is completely suppressed. In Figs. 8(c) and 8(d), the behavior of the parameters $\sigma_{12}/t_c = \sigma_{13}/t_c$ and the respective layer occupation numbers are shown. It is evident that for different $k_B T/t_c$ values, both parameters remain nearly constant and show no significant variation with increasing $k_B T/t_c$.

F. Phase diagrams: case $|J_K| > |J_H|$

The phase diagrams of $k_B T/t_c$ versus t_{13}/t_c in the case where $|J_K| > |J_H|$ are shown in Fig. 9. In this case, *layer 1* interacts with *layer 2* with a finite value of $t_{12}/t_c = 0.4$. At low values of t_{13}/t_c and as $k_B T/t_c$ decreases, the presence of a continuous transition (continuous black lines) from NS to $AF_c + K$ is observed. At low values of $k_B T/t_c$ and as the interaction between *layer 1* and *layer 3* increases, discontinuous transition (dashed black lines) from $AF_c + K$ to $F_c + K$ is observed. Subsequently, with the increase of t_{13}/t_c , a new discontinuous transition from $F_c + K$ to AF_c is shown. At high intensities of t_{13}/t_c

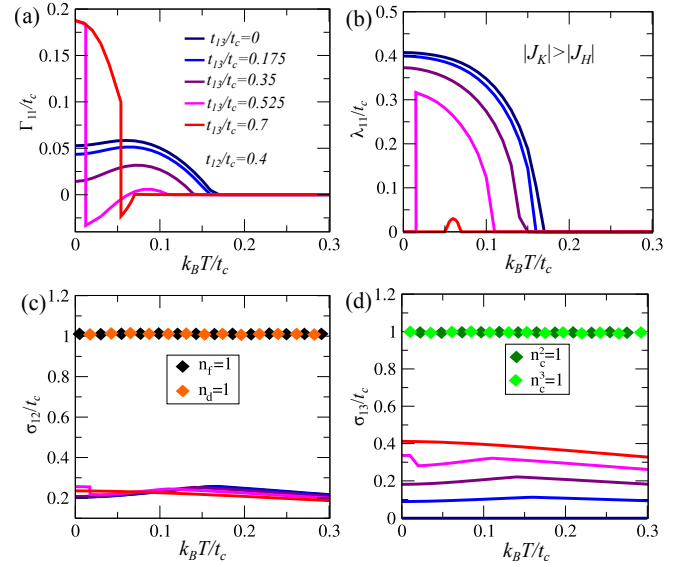


FIG. 7. Mean-field parameters (a) Γ_{11}/t_c , (b) λ_{11}/t_c , (c) σ_{12}/t_c and (d) σ_{13}/t_c as function of $k_B T/t_c$ under a variation of t_{13}/t_c for $n^f = 1$ and $n_t = (n_d + n_c^2 + n_c^3)/3 = 1$ in the case where the Heisenberg interaction is large compared to the Kondo coupling: $J_K = -0.5$, and $J_H = -0.1$. $W_{2(3)}^c = W^d = 1$ and the hopping parameter $t_{12}/t_c = 0.4$.

and with the increase of $k_B T/t_c$, a continuous transition between AF_c and NS is observed. Additionally, in Fig. 9(b) we show the phase diagram of T versus t_{13}/t_c in the case where $t_{12}/t_c = t_{13}/t_c$. The behavior of the phase diagram is similar to the previous one, see Fig. 6(a), where at low intensities of t_{13}/t_c and as $k_B T/t_c$ decreases, a continuous transition from NS to $AF_c + K$ is shown. Also, for low values of $k_B T/t_c$ and as t_{13}/t_c is increasing, a discontinuous transition from $AF_c + K$ to $F_c + K$, followed by a discontinuous transition from $F_c + K$ to AF_c .

IV. CONCLUSION AND EXPERIMENTAL EVIDENCE

In this work, we investigated the effects of interfacial proximity in a heterostructure displaying the Kondo effect and short-range magnetic correlations. Our heterostructure comprises three layers, where the first layer (*layer 1*) is governed by KHL model involving f - and d - electrons interacting via Kondo and Heisenberg couplings. The other two layers (*layer 2* and *3*) consist of non-interacting itinerant c -electrons, where the coupling to KHL is defined by two perpendicular hopping terms, t_{12}/t_c and t_{13}/t_c . Additionally, we have proposed two possible cases: $|J_K| < |J_H|$ and $|J_K| > |J_H|$, at *half-band filling*. We demonstrate that by varying t_{12}/t_c and t_{13}/t_c , electronic dynamics are induced at the KHL interface, altering the behavior of the mean-field parameters describ-

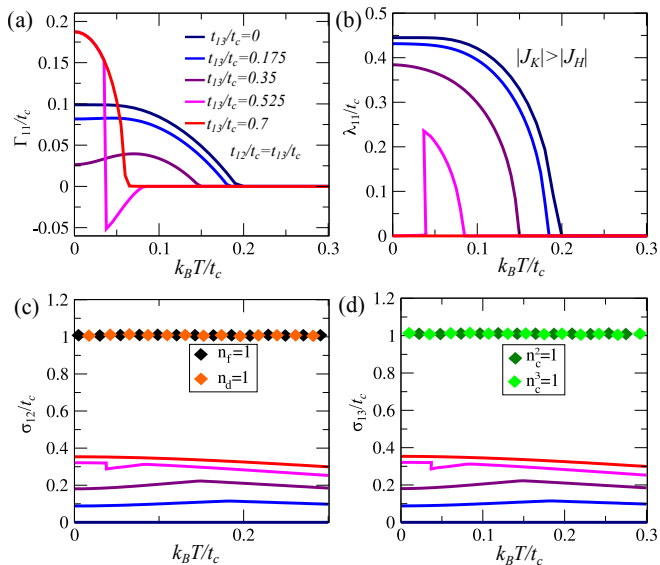


FIG. 8. Mean-field parameters (a) Γ_{11}/t_c , (b) λ_{11}/t_c , (c) σ_{12}/t_c and (d) σ_{13} as function of $k_B T/t_c$ under a variation of t_{13}/t_c for $n^f = 1$ and $n_t = (n_d + n_c^2 + n_c^3)/3 = 1$ in the case where the Heisenberg interaction is large compared to the Kondo coupling: $J_K = -0.5$, and $J_H = -0.1$. $W_{2(3)}^c = W_d = 1$ and the hopping parameters are $t_{12}/t_c = t_{13}/t_c$.

ing the Kondo effect (λ_{11}/t_c) and short-range magnetic correlations (Γ_{11}/t_c). In the case where $|J_K| < |J_H|$, AF_c are shown to dominate in the phase diagram of $k_B T/t_c$ versus t_{12}/t_c when the distance between layers is symmetric, $t_{12}/t_c = t_{13}/t_c$. Additionally, a *dome* is observed where K coexist with AF_c when the distances between layer interfaces are different, i.e., $t_{12}/t_c \neq t_{13}/t_c$. In the case where $|J_K| > |J_H|$, a sequence of discontinuous and continuous transitions is shown to evolve in the $k_B T/t_c$ versus t_{13}/t_c phase diagrams, with the formation of regions of pure AF_c , as well as regions of coexistence of $AF_c + K$ and $F_c + K$. This case shows a rich phase diagrams with a mixture of K and short-range magnetic correlations of different nature: AF_c and F_c . Through both cases, we propose that by alternatively studying the proximity effects between the interfaces in a Kondo-Heisenberg lattice and two metallic lattices, we can obtain Kondo and magnetic correlations, to those found in studies conducted outside of *half-filling* regime in compounds such as $CeCu_6$, $CeInCu_2$ and $CeRu_2Si_2$ [47–50].

The approach carried out with heterostructures could be an alternative route to study the *Nozières exhaustion problem*. This classic problem arises when there are not enough conduction electrons in the lattice to screen all spins of localized electrons in a two-dimensional Kondo lattice [44]. We speculate that by varying the interlayer hopping terms of the Kondo heterostructure, we can induce tunneling of conduction electrons, between layers, capable of screening the localized spins in the KHL.

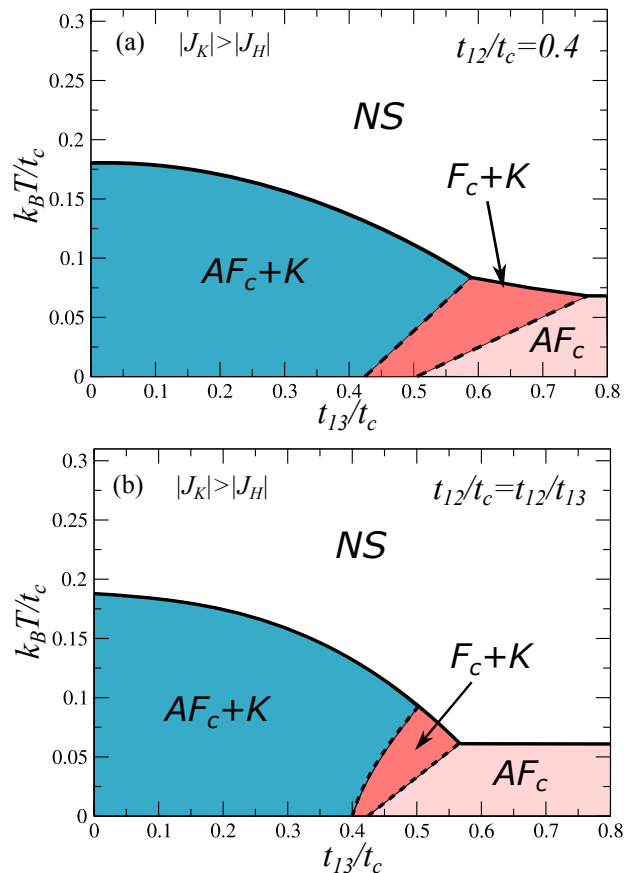


FIG. 9. Phase diagrams of $k_B T/t_c$ versus t_{13}/t_c with (a) $t_{12}/t_c = 0.4$ and (b) $t_{12}/t_c = t_{13}/t_c$ in the case where the Heisenberg interaction is large compared to the Kondo coupling: $J_K = -0.5$, and $J_H = -0.1$. $W_{2(3)}^c = W_d = 1$. NS is a normal state, AF_c are antiferromagnetic correlations, F_c are ferromagnetic correlations and K is a Kondo state. The continuous black lines are second-order transitions and the dashed black lines are first-order transitions.

ACKNOWLEDGMENTS

J. Faúndez, L. C. Prauchner and S. G. Magalhães thank the CNPq (Conselho Nacional de Desenvolvimento Científico e Tecnológico), processo: 200778/2022-6. J. Faúndez also acknowledges partial support from ANID Fondecyt grant number 3240320. S. E. Reyes-Lillo acknowledges support from ANID Fondecyt Regular grant number 1220986. Powered@NLHPC: This research was partially supported by the supercomputing infrastructure of the NLHPC (ECM-02). The authors would like to thank Miguel Gusmão for his valuable contribution during the discussions.

Appendix A: Green's Function

The Greens functions obtained from the equation of motion method (Zubarev formalism [51]) are given in the matrix representation as

$$-\langle\langle\Psi_{\mathbf{k}\sigma} \otimes \Psi_{\mathbf{k}\sigma}^\dagger\rangle\rangle_z = (z - \mathbf{h}_{\mathbf{k}})^{-1}. \quad (\text{A1})$$

Therefore, the minimum necessary set of Green's function is explicitly given as

$$\langle\langle f_{\mathbf{k}1\sigma} : f_{\mathbf{k}1\sigma}^\dagger \rangle\rangle_z = -\frac{-t_{d1c3}^2 (z - \epsilon_{c,2}(\mathbf{k})) + [(z - \epsilon_{d,1}(\mathbf{k})) (z - \epsilon_{c,2}(\mathbf{k})) - t_{d1c2}^2] (z - \epsilon_{c,3}(\mathbf{k}))}{D_3(\mathbf{k}, z)}, \quad (\text{A2})$$

$$\langle\langle d_{\mathbf{k}1\sigma} : f_{\mathbf{k}1\sigma}^\dagger \rangle\rangle_z = -\frac{2J_k \lambda_{11} (z - \epsilon_{c,2}(\mathbf{k})) (z - \epsilon_{c,3}(\mathbf{k}))}{D_3(\mathbf{k}, z)}, \quad (\text{A3})$$

$$\langle\langle d_{\mathbf{k}1\sigma} : d_{\mathbf{k}1\sigma}^\dagger \rangle\rangle_z = -\frac{(z - B\epsilon_{d,1}(\mathbf{k}) - E_0) (z - \epsilon_{c,2}(\mathbf{k})) (z - \epsilon_{c,3}(\mathbf{k}))}{D_3(\mathbf{k}, z)}, \quad (\text{A4})$$

$$\langle\langle c_{\mathbf{k}2\sigma} : c_{\mathbf{k}2\sigma}^\dagger \rangle\rangle_z = -\frac{-t_{d1c3}^2 (z - B\epsilon_{d,1}(\mathbf{k}) - E_0) + [(z - B\epsilon_{d,1}(\mathbf{k}) - E_0) (z - \epsilon_{d,1}(\mathbf{k})) - 4J_K^2 \lambda_{11}^2] (z - \epsilon_{c,3}(\mathbf{k}))}{D_3(\mathbf{k}, z)}, \quad (\text{A5})$$

$$\langle\langle c_{\mathbf{k}3\sigma} : c_{\mathbf{k}3\sigma}^\dagger \rangle\rangle_z = -\frac{-t_{d1c2}^2 (z - B\epsilon_{d,1}(\mathbf{k}) - E_0) + [(z - B\epsilon_{d,1}(\mathbf{k}) - E_0) (z - \epsilon_{d,1}(\mathbf{k})) - 4J_K^2 \lambda_{11}^2] (z - \epsilon_{c,2}(\mathbf{k}))}{D_3(\mathbf{k}, z)}, \quad (\text{A6})$$

$$\langle\langle d_{\mathbf{k}1\sigma} : c_{\mathbf{k}2\sigma}^\dagger \rangle\rangle_z = -\frac{(z - \epsilon_{c,2}(\mathbf{k})) (z - B\epsilon_{d,1}(\mathbf{k}) - E_0) t_{d1c2}}{D_3(\mathbf{k}, \omega)}, \quad (\text{A7})$$

$$\langle\langle d_{\mathbf{k}1\sigma} : c_{\mathbf{k}3\sigma}^\dagger \rangle\rangle_z = -\frac{(z - \epsilon_{c,3}(\mathbf{k})) (z - B\epsilon_{d,1}(\mathbf{k}) - E_0) t_{d1c3}}{D_3(\mathbf{k}, \omega)}, \quad (\text{A8})$$

where

$$D_3(\mathbf{k}, z) = [(z - \epsilon_{d,1}(\mathbf{k})) (z - \epsilon_{c,2}(\mathbf{k})) (z - \epsilon_{c,3}(\mathbf{k})) - t_{d1c2}^2 (z - \epsilon_{c,3}(\mathbf{k})) - t_{d1c3}^2 (z - \epsilon_{c,2}(\mathbf{k}))] (z - B\epsilon_{d,1}(\mathbf{k}) - E_0) - 4J_k^2 \lambda_{11}^2 (z - \epsilon_{c,2}(\mathbf{k})) (z - \epsilon_{c,3}(\mathbf{k})). \quad (\text{A9})$$

-
- [1] M. Naritsuka, S. Nakamura, Y. Kasahara, T. Terashima, R. Peters, and Y. Matsuda, Coupling between the heavy-fermion superconductor CeCoIn₅ and the antiferromagnetic metal CeIn₃ through the atomic interface, *Phys. Rev. B* **100**, 024507 (2019).
- [2] B. Zhou, S. Misra, E. da Silva Neto, P. Aynajian, R. E. Baumbach, J. D. Thompson, E. D. Bauer, and A. Yazdani. Visualizing nodal heavy fermion superconductivity in CeCoIn₅. *Nature Phys* **9**, 474–479 (2013).
- [3] P. J. W. Moll, T. Helm, S.-S. Zhang, C. D. Batista, N.

- Harrison, R. D. McDonald, L. E. Winter, B. J. Ramshaw, M. K. Chan, F. F. Balakirev, B. Batlogg, E. D. Bauer, and F. Ronning, Emergent magnetic anisotropy in the cubic heavy-fermion metal CeIn₃, *npj Quant Mater* **2**, 46 (2017).
- [4] A. K. Geim and I. V. Grigorieva, Van der Waals heterostructures, *Nature* **499**, 419 (2013).
- [5] Y. Liu, N. O. Weiss, X. Duan, H.-C. Cheng, Y. Huang, and X. Duan, Van der Waals heterostructures and devices, *Nat. Rev. Mater.* **1**, 1 (2016).

- [6] D. Jariwala, T. J. Marks, and M. C. Hersam, Mixed-dimensional van der Waals heterostructures, *Nature mater.* **16**, 170 (2017).
- [7] A.C. Lausmann, E.J. Calegari, Julián Faúndez, P.S. Riseborough, S.G. Magalhaes, Magnetic transitions induced by pressure and magnetic field in a two-orbital f -electron model in cubic and tetragonal lattices, *J. Magn. Magn. Mater.* **560** 169531 (2022).
- [8] J. K. Hyun, S. Zhang, and L. J. Lauhon, Nanowire Heterostructures, *Annu. Rev. Mater. Res.* **43**, 451 (2013).
- [9] J. H. Bang, M. S. Choi, A. Mirzaei, W. Oum, S. Han, S. S. Kim, and H. W. Kim, Porous Si/SnO₂ nanowires heterostructures for H₂S gas sensing, *Ceram. Int.* **46**, 604 (2020).
- [10] K. Willa, F. Hardy, D. Aoki, D. Li, P. Wiecek, G. Lapertot, and C. Meingast, Thermodynamic signatures of short-range magnetic correlations in UTe₂, *Phys. Rev. B* **104**, 205107 (2021).
- [11] J. Faúndez, S. G. Magalhaes, E. J. Calegari, and P. S. Riseborough, Multicritical points in a model for 5 f -electron systems under pressure and magnetic field, *J. Phys.: Condens. Matter* **33** 295801 (2021).
- [12] J. Faúndez, S. G. Magalhães, P. S. Riseborough, and S. E. Reyes-Lillo, Effect of a flat band on a multiband two-dimensional Lieb lattice with intra- and interband interactions, *J. Phys.: Condens. Matter* **36** 195601 (2024).
- [13] P. Zubko, S. Gariglio, M. Gabay, P. Ghosez, and J.-M. Triscone, Interface Physics in Complex Oxide Heterostructures, *Annu. Rev. Condens. Matter Phys.* **2**, 141 (2011).
- [14] Y. Cao, V. Fatemi, S. Fang, K. Watanabe, T. Taniguchi, E. Kaxiras, and P. Jarillo-Herrero, Correlated insulator behaviour at half-filling in magic-angle graphene superlattices, *Nature* **556**, 43 (2018).
- [15] R. Bistritzer and A. H. MacDonald, Moiré bands in twisted double-layer graphene, *PNAS* **108**, 12233 (2011).
- [16] J. Szeftel, N. Sandeau, M. Abou Ghantous, and M. El Saba, Towards room-temperature superconductivity, *EPL* **134**, 27002 (2021).
- [17] V. A. Posey, S. Turkel, M. Rezaee, A. Devarakonda, A. K. Kundu, C. S. Ong, M. Thinel, D. G. Chica, R. A. Vitalone, R. Jing, S. Xu, D. R. Needell, E. Meirzadeh, M. L. Feuer, A. Jindal, X. Cui, T. Valla, P. Thunström, T. Yilmaz, E. Vescovo, D. Graf, X. Zhu, A. Scheie, A. F. May, O. Eriksson, D. N. Basov, C. R. Dean, A. Rubio, P. Kim, M. E. Ziebel, A. J. Millis, A. N. Pasupathy, and X. Roy, Two-dimensional heavy fermions in the van der Waals metal CeSiI. *Nature* **625**, 483–488 (2024).
- [18] V. Palankovski and R. Quay, Analysis and simulation of heterostructure devices (Springer Science and Business Media, 2004).
- [19] H. Kroemer, in *Electronic Structure of Semiconductor Heterojunctions* (Springer, 1988) pp. 116–149.
- [20] R. Yan, G. Khalsa, S. Vishwanath, Y. Han, J. Wright, S. Rouvimov, D. S. Katzer, N. Nepal, B. P. Downey, D. A. Muller, Huili G. Xing, David J. Meyer, and Debdeep Jena, GaN/NbN epitaxial semiconductor/superconductor heterostructures, *Nature* **555**, 183 (2018).
- [21] G. Mazza, A. Amaricci, and M. Capone, Interface and bulk superconductivity in superconducting heterostructures with enhanced critical temperatures, *Phys. Rev. B* **103**, 094514 (2021).
- [22] K. Yasuda, R. Wakatsuki, T. Morimoto, R. Yoshimi, A. Tsukazaki, K. Takahashi, M. Ezawa, M. Kawasaki, N. Nagaosa, and Y. Tokura, Geometric Hall effects in topological insulator heterostructures, *Nature Phys.* **12**, 555 (2016).
- [23] M. Zhu, H. Hu, S. Cui, Y. Li, X. Zhou, Y. Qiu, R. Guo, G. Wu, G. Yu, and H. Zhou, Strain-driven radial vortex core reversal in geometric confined multiferroic heterostructures, *Appl. Phys. Lett.* **118**, 262412 (2021).
- [24] D. Bimberg, M. Grundmann, and N. N. Ledentsov, Quantum dot heterostructures (John Wiley and Sons, 1999).
- [25] Z. H. Liu, B. Frank, L. Janssen, M. Vojta, and F. F. Assaad, Magnetic quantum phase transition in a metallic Kondo heterostructure, *Phys. Rev. B* **107**, 165104 (2023).
- [26] V. Vaño, M. Amini, S. C. Ganguli, G. Chen, J. L. Lado, S. Kezilebieke, and P. Liljeroth, Artificial heavy fermions in a van der Waals heterostructure. *Nature* **599**, 582–586 (2021).
- [27] H. Shishido, T. Shibauchi, K. Yasu, T. Kato, H. Kontani, T. Terashima, and Y. Matsuda, Tuning the Dimensionality of the Heavy Fermion Compound CeIn₃, *Science* **327**, 980-983 (2010).
- [28] E. Huecker and Y. Komijani, Spin fractionalization in a Kondo-lattice superconductor heterostructure, *Phys. Rev. B* **108**, 195120 (2023).
- [29] F. Yang, Z. Wang, Y. Liu, S. Yang, Z. Yu, Q. An, Z. Ding, F. Meng, Y. Cao, Q. Zhang, L. Gu, M. Liu, Y. Li, J. Guo, and X. Liu, Engineered Kondo screening and nonzero Berry phase in SrTiO₃/LaTiO₃/SrTiO₃ heterostructures, *Phys. Rev. B* **106**, 165421 (2022).
- [30] Ed. Martino, C. Putzke, M. König, P. J. W. Moll, H. Berger, D. LeBoeuf, M. Leroux, C. Proust, A. Akrap, H. Kirmse, C. Koch, S. Zhang, Q. Wu, O. V. Yazyev, L. Forró, and K. Semeniuk, Unidirectional Kondo scattering in layered NbS₂, *npj 2D Mater Appl* **5**, 86 (2021).
- [31] A. Euverte, F. Hebert, S. Chiesa, R. T. Scalettar, and G. G. Batrouni, Kondo Screening and Magnetism at Interfaces, *Phys. Rev. Lett.* **108**, 246401 (2012).
- [32] R. G. Endres, D. L. Cox, R. R. P. Singh, and S. K. Pati, Mediation of Long Range Charge Transfer by Kondo Bound States, *Phys. Rev. Lett.* **88**, 166601 (2002).
- [33] H. Liu, Y. Xue, J.-A. Shi, R. A. Guzman, P. Zhang, Z. Zhou, Y. He, C. Bian, L. Wu, R. Ma, J. Chen, J. Yan, H. Yang, C.-M. Shen, W. Zhou, L. Bao, and H.-J. Gao, Observation of the Kondo Effect in Multilayer Single-Crystalline VTe₂ Nanoplates, *Nano Lett.* **19**, 12 (2019).
- [34] A. Allerdt, A. E. Feiguin, and S. Das Sarma, Competition between Kondo effect and RKKY physics in graphene magnetism, *Phys. Rev. B* **95**, 104402 (2017).
- [35] R. Peters, Y. Tada, and N. Kawakami, Magnetism in f -electron superlattices, *Phys. Rev. B* **94**, 205142 (2016).
- [36] Z.-P. Shi, R. R. P. Singh, and B. M. Klein, Interlayer Magnetic Coupling in Magnetic/Kondo Lattice Multilayered Structures, *Europhysics Letters* **29**, 7 (1995).
- [37] J. Yang, Q. Wang, T. Ma, and Q. Chen, Degenerate orbital effect in a three-orbital periodic Anderson model, *Phys. Rev. B* **99**, 245136 (2019).
- [38] M. Naritsuka, T. Terashima, and Y. Matsuda, Controlling unconventional superconductivity in artificially engineered f -electron Kondo superlattices, *J. Phys.: Condens. Matter* **33**, 273001 (2021).
- [39] J. R. Iglesias, C. Lacroix, and B. Coqblin, Revisited Dornich diagram: Influence of short-range antiferromag-

- netic correlations in the Kondo lattice, *Phys. Rev. B* **56**, 11820 (1997).
- [40] A. R. Ruppenthal, J. R. Iglesias, and M. A. Gusmao, Effect of band filling in the Kondo lattice: A mean-field approach, *Phys. Rev. B* **60**, 7321 (1999).
- [41] B. H. Bernhard and C. Lacroix, Coexistence of magnetic order and Kondo effect in the Kondo-Heisenberg model, *Phys. Rev. B* **92**, 094401 (2015).
- [42] S. A. dos Anjos Sousa-Júnior, J. P. de Lima, N. C. Costa, and R. R. dos Santos, Superconducting Kondo phase in an orbitally separated bilayer, *Phys. Rev. Research* **2**, 033168 (2020).
- [43] R. Peters, Y. Tada, and N. Kawakami, Kondo effect in f -electron superlattices, *Phys. Rev. B* **88**, 155134 (2013).
- [44] P. Nozières, Some comments on Kondo lattices and the Mott transition, *Eur. Phys. J. B*, **6**, 447 (1998).
- [45] B. Coqblin, C. Lacroix, M. A. Gusmao, J. R. Iglesias, Band-filling effects on Kondo-lattice properties, *Phys. Rev. B* **67**, 064417 (2003).
- [46] R. Cai, I. Žutić, W. Han, Superconductor/Ferromagnet Heterostructures: A Platform for Superconducting Spintronics and Quantum Computation. *Adv. Quantum Technol.* **6**, 2200080 (2022).
- [47] J. Rossat-Mignot, L. P. Regnault, J. L. Jacoud, C. Vettier, P. Lejay, J. Flouquet, E. Walker, D. Jaccard, and A. Amato, *J. Magn. Magn. Mater.* **76-77**, 376 (1988).
- [48] L. P. Regnault, W. A. C. Erkelens, J. Rossat-Mignod, P. Lejay, and J. Flouquet, *Phys. Rev. B* **38**, 4481 (1988).
- [49] J. Pierre, P. Haen, C. Vettier, and S. Pujol, *Physica B* **163**, 463 (1990).
- [50] H. V. Lihnneysen, S. Mock, A. Neubert, T. Pietrus, A. Rosh, A. Schroder, O. Stockert, and U. Tutsch, Heavy-fermion systems at the magnetic-nonmagnetic quantum phase transition, *J. Magn. Magn. Mater.* **177-181**, 12 (1998).
- [51] D. N. Zubarev, Double-time Green functions in statistical physics, *Sov. Phys. Usp.* **3** 320 (1960).